Research on Engineering Structures & Materials
www.jresm.org
MIM Research Group

Research Article

Experimental and numerical investigation of the cyclic behavior of masonry walls with a precise interlock brick system

Elfiranahla Chandra Dewi [1,a], Yosafat Aji Pranata [*,2,b], Chusla Ramah Darmawan [1,c], Ratnawati [1,d], Yelmi Arya Putra [3,e], Zulfikar [3,f]

[1]*Research and Development Department, PT Semen Indonesia (Persero) Tbk (SIG), Indonesia*
[2]*Master Program in Civil Engineering, Universitas Kristen Maranatha, Indonesia*
[3]*Non-Cement Business and Derivative Products Department, PT Semen Padang, Indonesia*

Article Info

Article History:

Received 25 July 2026
Accepted 17 Oct 2026

Keywords:

PIB;
Strength;
Stiffness;
Cyclic;
Behavior

Abstract

This study evaluates the cyclic behavior of a full-scale, two-dimensional in-plane Precise Interlock Brick (PIB) wall prototype (3000 × 3000 mm) through experimental testing and numerical analysis. Experimental tests were conducted under cyclic loading in accordance with ASTM E2126-19, while nonlinear finite element analysis and pushover simulations were performed to develop capacity curves. The investigation focused on lateral load capacity, ductility, initial and post-elastic stiffness, and energy dissipation. The seismic demand curve was established based on the Indonesian earthquake map. The numerical results demonstrated trends consistent with the experimental findings, although the predicted maximum load capacity (82.80 kN) was 18.93% lower than the experimentally measured value (102.14 kN). The prototype exhibited a ductility factor of 2.17, indicating limited-to-moderate ductility, and an energy dissipation capacity of 30,382.73 kN·mm. The findings provide empirical data on the strength and stiffness characteristics of PIB walls, supporting the development and calibration of design-oriented analytical models and their integration into three-dimensional structural analyses. Furthermore, the demand-to-capacity ratio (DCR) results indicate that the tested prototype satisfies the adopted strength criterion for design spectral acceleration values (SDS) of up to 0.80g. Overall, PIB technology offers a promising solution for rapid and efficient housing construction while maintaining structural performance in accordance with design standards.

© 2026 MIM Research Group. All rights reserved.

1. Introduction

A community's basic requirement is housing, and as Indonesia's population grows, so does the country's housing needs. This disparity between the availability and demand for housing frequently results in issues like overcrowding, the expansion of informal settlements, and a drop in living standards. As a result, addressing housing requirements necessitates concerted efforts from the public and commercial sectors as well as communities. These efforts include legislation for affordable housing, sustainable urban design, and easier access to funding.

Compared to traditional homes, residential buildings made primarily of interlocking brick provide consumers with the benefit of quick construction. Other benefits include being seismic and ecologically friendly, as well as having very affordable rates [1, 2]. Buildings made with environmentally friendly concrete are still being built [3, 4]. The interlocking wall structure has

*Corresponding author: yosafat.ap@maranatha.ac.id
[a]orcid.org/ 0009-0001-3019-7217; [b]orcid.org/0000-0002-7828-124X; [c]orcid.org/0009-0009-7452-3705; [d]orcid.org/0009-0001-3223-9134; [e]orcid.org/0009-0001-7615-7173; [f]orcid.org/0009-0008-3981-3881
DOI: http://dx.doi.org/10.17515/resm2026-2041ea0725rs

outstanding performance against impact and lateral stresses, according to several prior experiments. The findings of a study on the behavior of the lightweight interlocking brick system were reported by Rasidi et al. [5]. The findings of a study on the dynamic response of a reinforced interlocking brick wall under impact loading were reported by Wang et al. [6]. Meeting the strength and stiffness behavior requirements outlined in the codes is part of the problem formulation process for earthquake-resistant building design [7, 8, 9]. A research gap remains in the limited application of numerical modeling for interlocking wall system structures, particularly using the finite element method (FEM). This approach is crucial as a preliminary analytical tool to predict the strength and stiffness capacity of such systems prior to prototype fabrication and experimental testing in the laboratory.

This research aims to evaluate the cyclic behavior of a two-dimensional in-plane wall Precise Interlock Brick (PIB) prototype through numerical analysis and experimental testing. The research adopts an experimental approach to obtain the strength and stiffness under cyclic loading. Numerical analysis is performed to model the 2D specimens and develop capacity curves using pushover analysis.

The hypothesis proposes that the interlocking wall contributes significantly to the overall lateral stiffness of the structure. The stiffness contribution of the wall should be explicitly considered in the structural modeling of frame systems, particularly when defining the effective stiffness of the structural members and their interaction with the wall. To investigate this hypothesis, the research adopts a combined experimental and numerical approach. To gather empirical information on the strength and stiffness behavior of a two-dimensional (2D) in-plane wall under cyclic loading, experimental testing was carried out. In parallel, pushover analysis is used to build the capacity curves of the 2D wall specimens and simulate their behavior. The dependability of the suggested wall stiffness and strength models and their suitability for depicting the wall contribution in three-dimensional structural modeling are next assessed by comparing the experimental and numerical results.

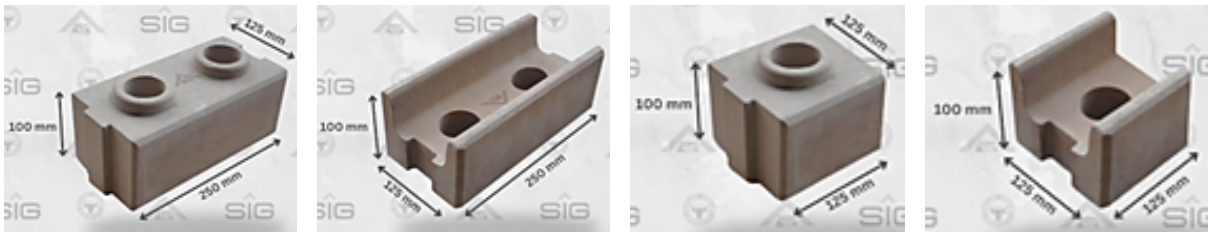
The scope of the study focuses on a full-scale 2D in-plane wall specimen measuring 3000 mm by 3000 mm. The behavior investigated includes capacity in terms of proportional and ultimate limits, ductility, initial and post-elastic stiffness, and energy dissipation. Experimental tests were conducted in the laboratory using cyclic loading in accordance with ASTM E2126-19 codes [10]. Numerical modeling was performed using the finite element method with pushover analysis to obtain the capacity curve using SAP2000 nonlinear [11], with mechanical properties of concrete and steel based on primary data obtained from previous studies [12, 13]. The design earthquake load (demand curve) used to evaluate the performance of the PIB prototype is based on the Indonesian earthquake map [14].

The novelty of this research is the creation of actual data on the in-plane strength and stiffness capability of a Precise Interlock Brick (PIB) wall prototype. These experimentally derived strength and stiffness characteristics provide a quantitative basis for characterizing the structural response of PIB walls and can be used to parameterize wall stiffness in three-dimensional structural models. The results therefore contribute both experimental evidence and practical modeling parameters for the integration of PIB wall systems into structural analysis and design.

Regarding sustainable composite material development, renewable and bio-derived material systems can be considered for use [15, 16]. An eco-friendly [17] building concept served as the foundation for the development of Precise Interlock Brick (PIB). PIB is made out of cement-sand bricks that are intended to replace traditional masonry units. Because these bricks are designed to interlock with one another, construction can be completed more quickly and effectively. Furthermore, because PIB doesn't need to be fired during manufacture, it is seen as environmentally beneficial [13]. The PIB system's materials are carefully chosen and adhere to predetermined quality criteria. The ecologically friendly Portland composite cement used as the binder was made in compliance with SNI 7064:2014 [18]. Natural (uncrushed) sand that has undergone physical testing in compliance with ASTM C33/C33M-23 is used as the fine aggregate [19].

Recent research has examined restricted masonry walls subjected to cyclic loading [20], cyclic confined masonry with apertures [21], and reinforced mortarless interlocking-brick walls evaluated under in-plane cyclic loading [22]. These studies show that loading history, reinforcement/confinement effects, stiffness deterioration, cracking, and other interacting factors control cyclic masonry response.

According to SNI T-15-1991-03 [23], the sand is free of organic contaminants that could lower the quality of concrete and has strong, resilient grains that range in size from 0.075 to 0.5 mm. Mud, oil, and other obvious impurities are absent from the mixing water, which is also colorless, odorless, and tasteless. Figure 1 and Figure. 2, which depict the type of interlocking bricks and a schematic 3D model of a PIB house with a plan dimension of 6 m by 6 m, respectively, provide examples of the PIB system.



(a) Type 1 (b) Type 2 (c) Type 3 (d) Type 4

Fig. 1. Type of interlock bricks [12]

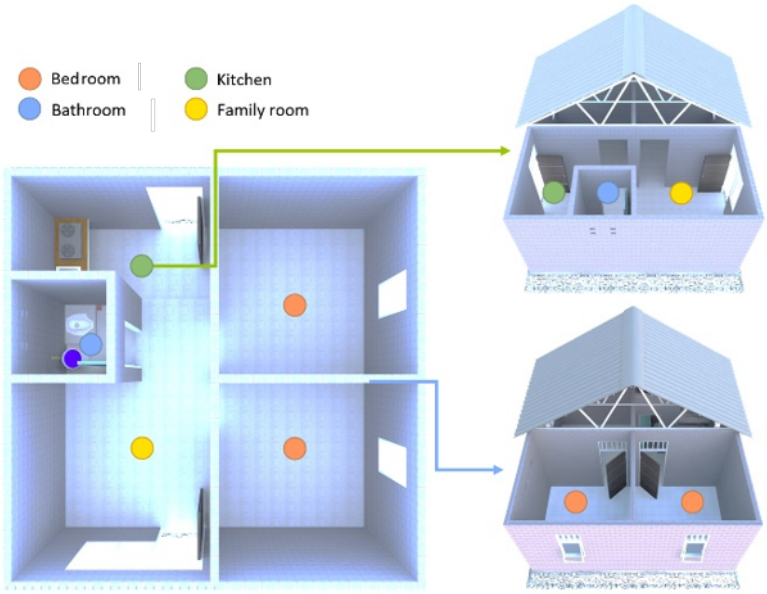


Fig. 2. Schematic 3D model of Precise Interlock Brick (PIB) house type of 6 m by 6 m [13]

2. Methods

This study employed an experimental method conducted in the laboratory to obtain empirical data on the capacity curve of specimens subjected to cyclic loading. The specimen consisted of a two-dimensional (2D) in-plane wall. The resulting capacity curve represents the relationship between shear force (lateral load) and specimen deformation under cyclic loading, in which the applied load is gradually increased until the specimen reaches its ultimate capacity and eventual failure. The loading protocol used in the experimental tests followed ASTM E2126-19 [10].

In addition, numerical analysis was performed using the nonlinear finite element method to model the two-dimensional specimens and to develop capacity curves through pushover analysis for verification purposes. To ensure model validity, the mechanical properties of the constituent materials, namely concrete and reinforcing steel, were defined based on data obtained from prior

material testing [12]. The two-dimensional wall system was modeled as a frame structure, with columns and beams representing the primary elements and steel reinforcement idealized as bracing components. The wall elements were not explicitly modeled; instead, their stiffness contribution was incorporated through parameterized inertia modifiers applied to the columns and beams.

2.1 Experimental Tests

Using full-scale test specimens, experimental testing utilizing a destructive loading approach was carried out to gather empirical data on the strength and stiffness behavior of the structural system. The specimens were generally subjected to incremental lateral stress in accordance with recommended loading procedures and pertinent testing standards, such as ASTM E2126-19 [10]. The loading method was continued through repeated displacement-controlled cycles until the specimens achieved their final capacity or failure condition. The test results yielded empirical lateral load-deformation relationships, which were then utilized to describe the specimens' total cyclic response, strength, and stiffness.

The parameters obtained from the test include load capacity and lateral displacement at the proportional limit, load capacity and lateral displacement at the ultimate limit state, ductility, initial stiffness, and post-elastic stiffness. The loading history was based on FEMA P-750 [24], with slight modifications, specifically the elimination of small cycles between drift levels, as shown in Figure 3, which presents the cyclic loading pattern used in the experimental testing. The drift ratio was calculated based on FEMA P-750, as expressed in Equation 1.

$$0.80 \leq 0.67\left(\frac{h_w}{l_w}\right) + 0.5 \leq 2.5 \tag{1}$$

where h_w is the height of specimen (3000 mm) and lw is the length of specimen (3000 mm).

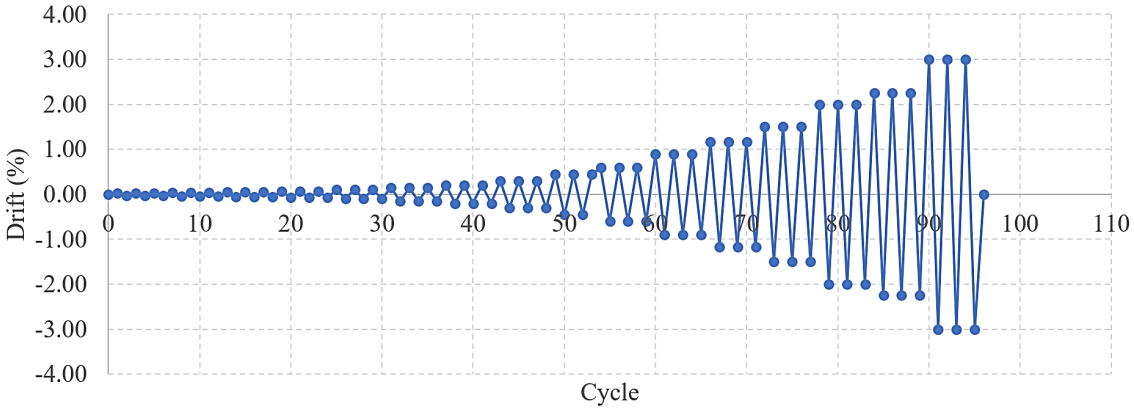


Fig. 3. Cyclic loading pattern for experimental tests

Cyclic loading tests (push–pull loading) are required to obtain energy dissipation parameters, which are essential for evaluating the performance of structural systems under lateral loads representing earthquake actions [25, 26, 27]. This experimental approach is increasingly adopted by researchers and engineers to investigate the strength and stiffness behavior of structures, including the failure and collapse mechanisms of test specimens [28, 29, 30].

2.2 Numerical Analysis

Finite element analysis (FEA) is a numerical method used to solve complex boundary value problems in engineering by discretizing a large domain into smaller, simplified elements connected at nodes. Various types of elements can be employed in this approach, including frame and beam elements [11, 31, 32].

Pushover analysis is a nonlinear static analysis method used to evaluate the capacity of a structure to resist lateral loads, such as earthquake actions, by incrementally applying horizontal loads until a target displacement or collapse condition is reached. This analysis produces a capacity curve

representing the relationship between base shear and roof displacement, which is used to identify plastic hinge formation and failure mechanisms. The method is increasingly adopted by engineers to assess structural performance under lateral loading [33, 34, 35]. Figure 4 illustrates the frame elements used to model columns and beams, while Figure 5 presents the plastic hinge property model employed in the nonlinear representation of frame elements.

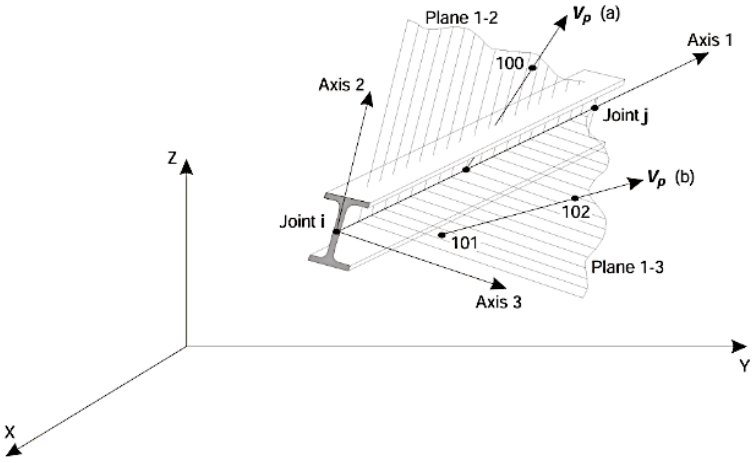


Fig. 4. The frame element local coordinate system [11]

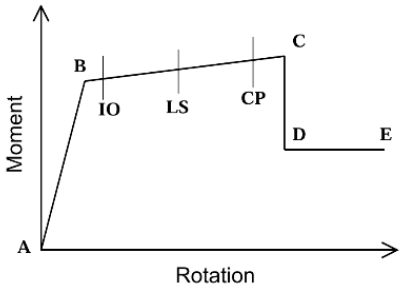


Fig. 5. The plastic hinge property model [11]

2.3 Demand versus Capacity (DCR) Ratio

In low-rise buildings, structural behavior is predominantly governed by strength. Strength evaluation is conducted by comparing the lateral load-carrying capacity of the system ($V_{capacity}$) with the seismic base shear force (V), which is determined based on the design earthquake in accordance with SNI 1726:2019 [7].

$$V = C_s W \tag{2}$$

where W is the effective seismic weight of structure (unit in kN) and C_s Seismic response coefficient determined according to SNI 1726:2019 codes [7].

The effective seismic weight is determined based on the assumption that the structural mass is concentrated at the roof level (lumped mass), and that the contributing weight of the structure is taken as half of the height of the vertical structural element and above. The distribution of seismic forces to each wall segment is calculated according to the tributary area supported by the respective wall element. The lateral resistance capacity is derived from the backbone curve obtained from experimental results, using an offset corresponding to the maximum lateral push–pull load that the structure can sustain prior to collapse. This value is then divided by the system overstrength factor (Ω_0 = 2.5) for the wall system [7]. Accordingly, the lateral resistance capacity represents the actual contribution of structural components in resisting lateral loads, without considering system redundancy. For evaluation purposes, the governing lateral capacity of the structure is taken as the minimum value between the push and pull capacities. A structural system is considered adequate in resisting earthquake actions when its lateral capacity ($V_{capacity}$) exceeds the seismic demand or base shear force (V).

3. Results and Discussion

3.1 Results of Experimental Tests

In this test, cyclic lateral loads were applied at the top of each specimen to assess its strength, stiffness, energy dissipation capability, and damage patterns. The specimens were permitted to experience in-plane deformation to approximate the lateral reaction of a structural wall under earthquake-induced loads. To determine the load-displacement response, the lateral load and associated displacement were continually monitored and recorded during the cyclic loading

process. The structural behavior, load-carrying capacity, stiffness degradation, energy dissipation capacity, and damage development of the specimens were all described using these experimental responses. The idea that the test specimens should accurately reflect the pertinent structural and loading conditions anticipated in a prototype structure subjected to earthquake-induced lateral loading guided the design and proportions of the specimens.

To ensure conservative results in the 2D wall cyclic testing, the selected wall segments corresponded to interior walls assumed to receive the largest tributary area loads (Figure 6). Likewise, the boundary frame configuration was designed conservatively in terms of both geometric dimensions and cross-sectional orientation. Figure 7 shows that the confined masonry wall is assumed to resist the majority of the seismic load; therefore, only the confined masonry wall component was used as the test specimen.

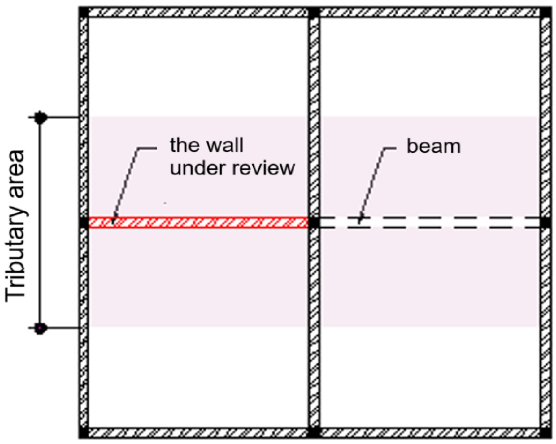


Fig. 6. Retrieval of the tested wall segment of house type of 6 m by 6 m [13]

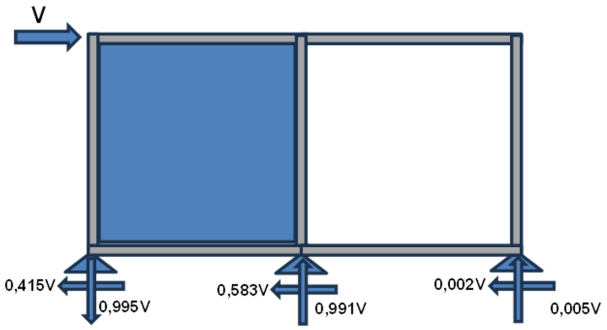


Fig. 7. Load distribution on walls and frames [13]

The test specimens generally consist of a wall restraint frame system (i.e., beams and columns), wall components, connections between structural elements, and connections between the superstructure and substructure, configured to represent actual field application conditions. A typical setup for 2D wall cyclic testing is illustrated in Figure 8.

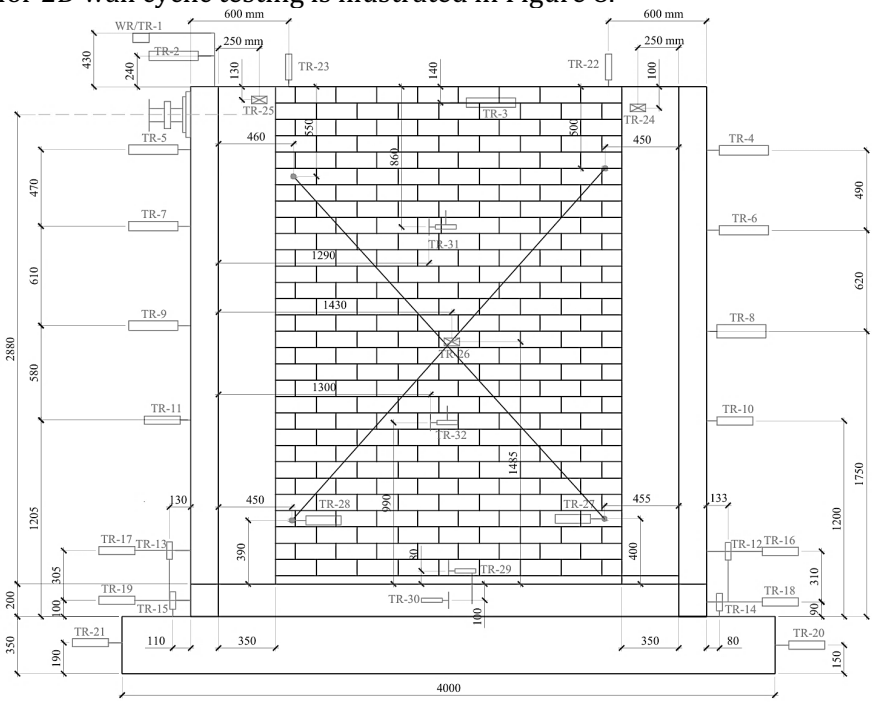


Fig. 8. Typical 2D wall in-plane cyclic testing setup [13]

The cyclic testing was conducted using a displacement-controlled loading protocol, in which lateral loads were applied alternately in the push and pull directions using a load cell with a maximum capacity of 200 kN. The target displacement was incrementally increased according to the prescribed loading history. To measure deformation, linear variable displacement transducers (LVDT) were installed at several locations, as shown in Figure 8.

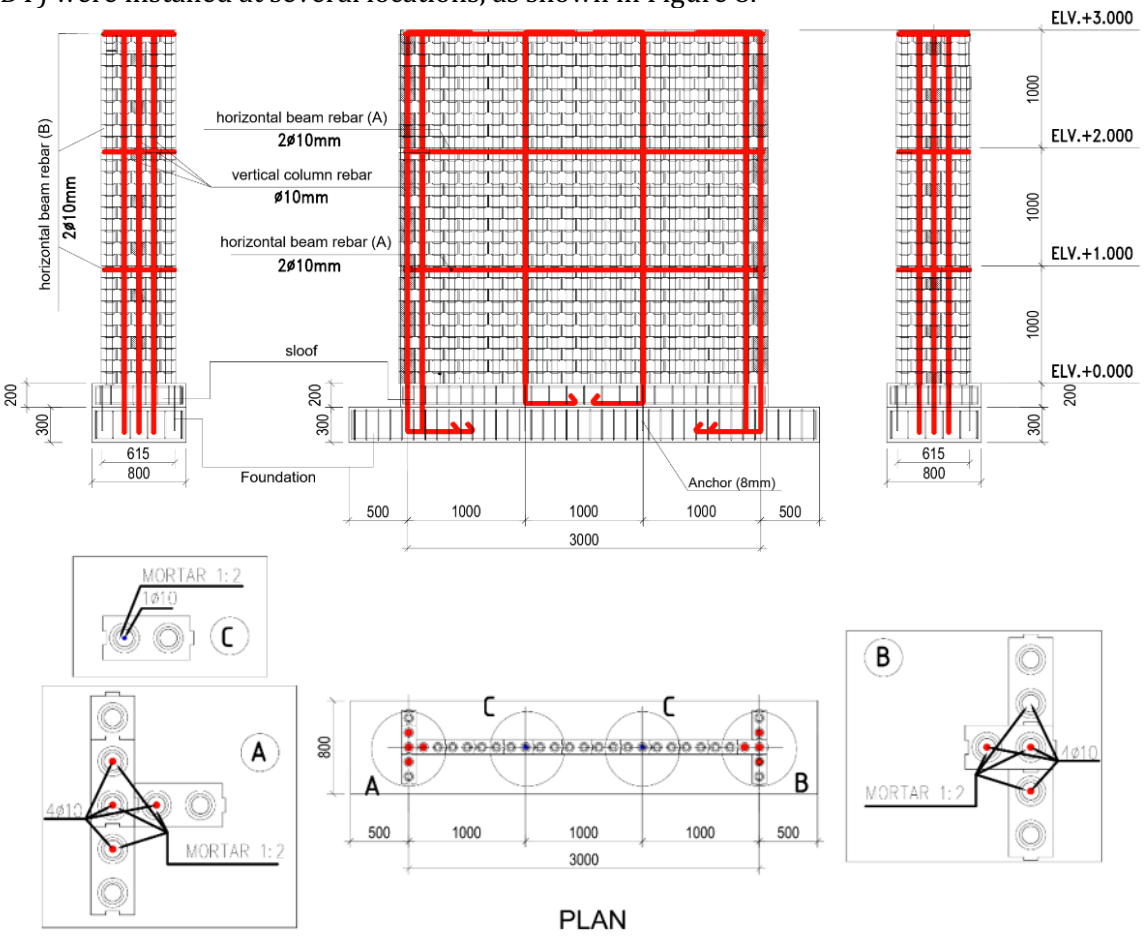


Fig. 9. Schematic 2D specimens detailing of PIB prototype [13]

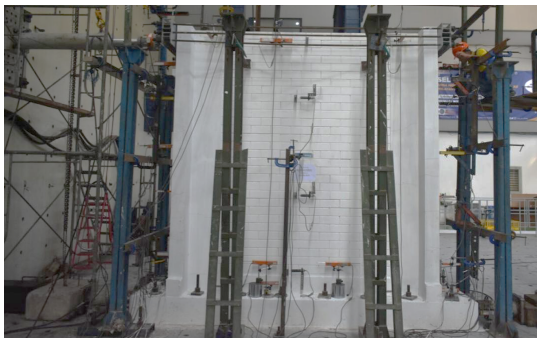


Fig. 10. Setup of PIB specimens

In this study, displacement was expressed in terms of drift ratio (percentage), defined as the lateral displacement divided by the height of the test specimen. Figure 9 shows the detailed configuration of the PIB prototype specimens [12, 13]. In this study, a single specimen was tested. The complete experimental results are presented in Figure 10, Figure 11, and Figure 12. Figure 10 illustrates the test setup of the specimen, while Figure 11 shows the observed wall failure patterns at drift ratios of 0.50% (Figure 11a) and 3.00% (Figure 11b), respectively.



(a) Drift 0.50% (b) Drift 3.00%

Fig. 11. The wall failure patterns that occurred in specimen

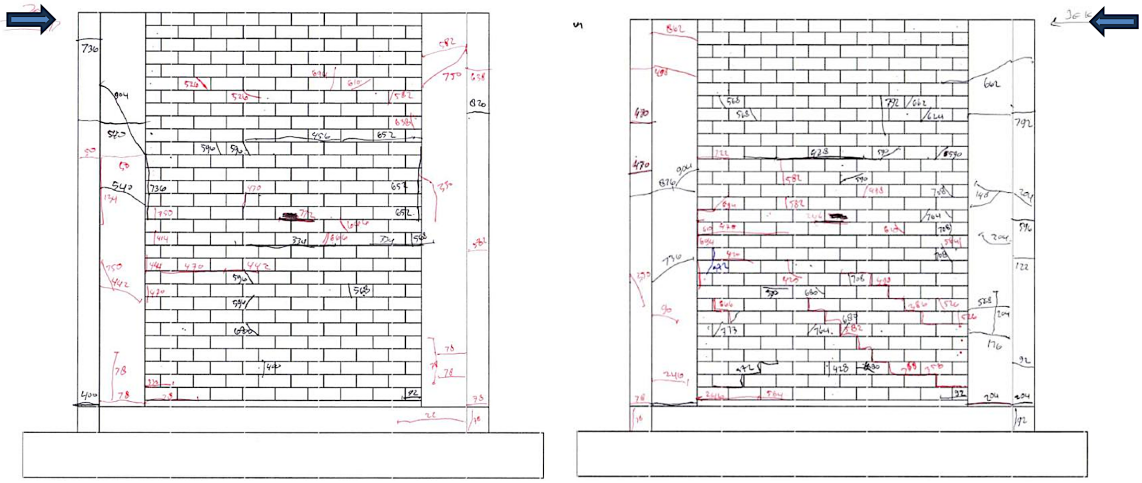


Fig. 12. Crack pattern due to push and pull loads (Drift 3.00%)

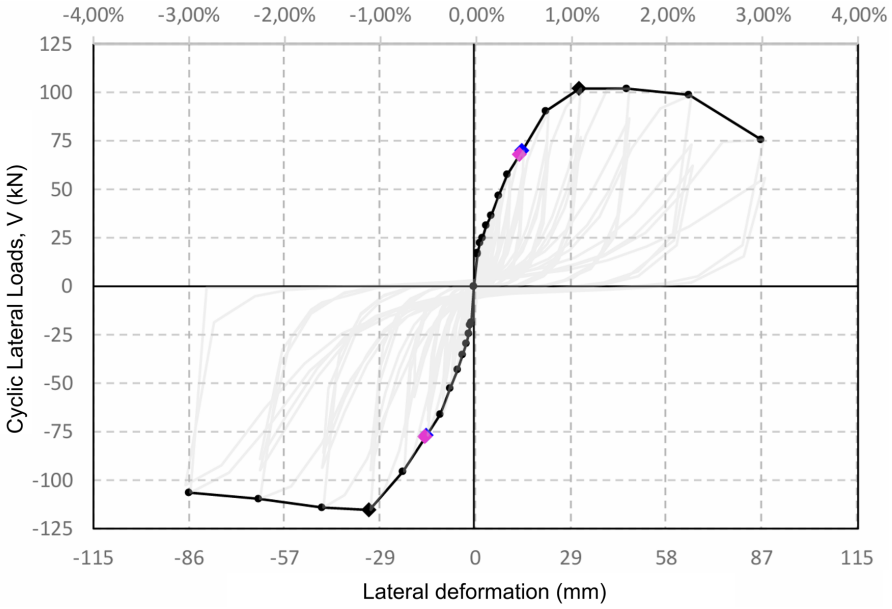
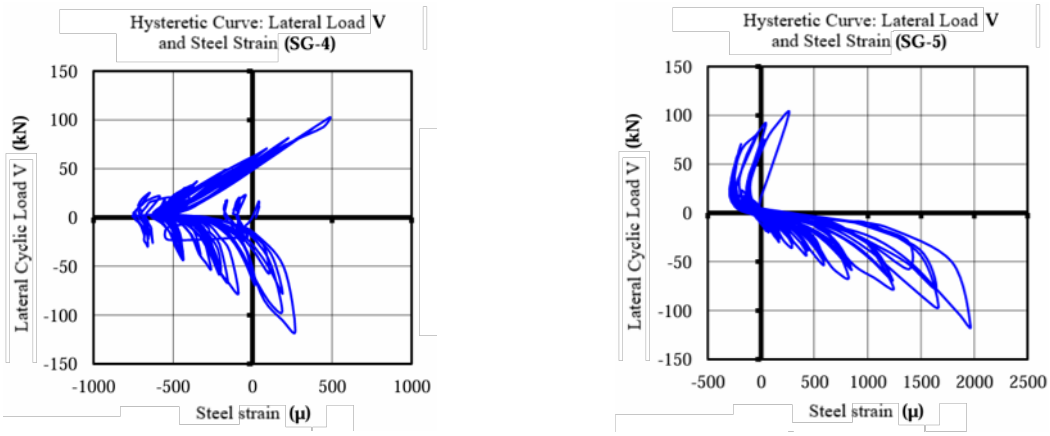


Fig. 13. The load-to-cyclic lateral deformation relationship curves obtained from experimental tests [13]

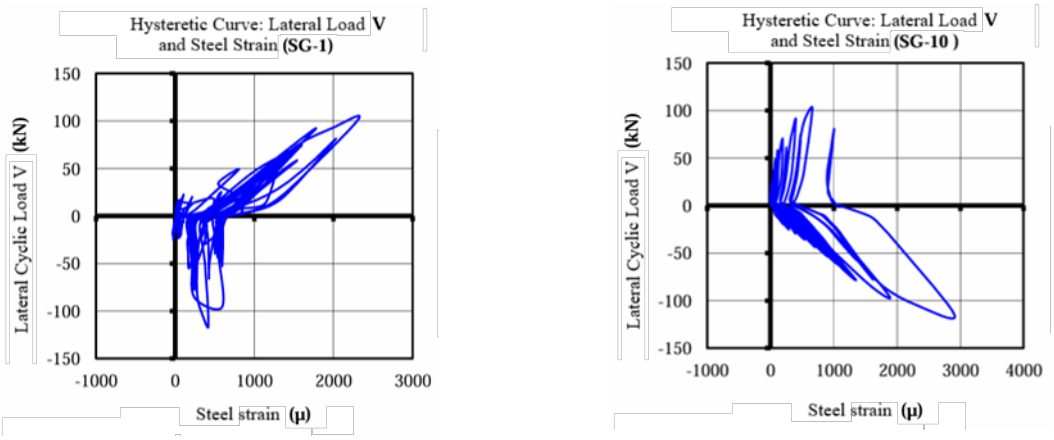
The maximum lateral push–pull load is limited to a drift ratio of 3.00%. Figure 12 presents the crack patterns under push and pull loading at a drift level of 3.00%, which is the observed crack evolution from initial formation until the end of the test. The significant yield point of the system was determined using the equivalent energy method. Deformation and damage progression during the

testing process were continuously monitored. At the peak of each loading cycle, cracks induced by the applied load were identified, mapped, and numbered according to the loading stage. Figure 12 presents the observed crack evolution from initial formation until the end of the test. Black lines represent cracks occurring under push (compressive) loading conditions, while red lines indicate cracks developing under pull (tensile) loading conditions.

Figure 13 presents the backbone curve of the test results, including key response points such as the yield point and maximum strength. In addition, the wall shear strength (V_{peak}) is evaluated by dividing $V_{maximum}$ by the wall length, following the procedure specified in ASTM E2126-19 [10]. Table 1 shows all of the results of the calculations for strength and stiffness capacity. The in-plane shear capacity of the wall is determined by dividing the maximum lateral push–pull load ($V_{maximum}$) by the structural overstrength factor (Ω_0).



(a) Lateral force and strain curves of mid-span rebar



(b) Lateral force and strain curves of end rebar

Fig. 14. Results of lateral force and strain curves of mid-span and end rebars [13]

Furthermore, reinforcement yielding (Ø10) was evaluated using strain gauges with a yield strain threshold of 1400 με, as shown in Figure 14. The results indicate that most reinforcement bars reached yielding conditions by the end of the test, as reflected by strain gauge readings at SG-1, SG-4, SG-5, and SG-10. Based on these measurements, reinforcement yielding was observed at a drift ratio of 0.35% and at 0.75%. Accordingly, the lateral load capacity of the wall system under push and pull loading is summarized in Table 1.

One of the factors that affects how well a structure performs under seismic loads is the energy dissipation capability of a component and structural system. When a structure is subjected to alternating loads, the energy it absorbs during a single loading cycle is equal to the total of the energy it absorbs during push and pull loads. The enclosed area inside the hysteresis curve loop is used to compute the energy dissipation for each cycle. The energy dissipation numbers from earlier

test cycles can then be added up to determine cumulative energy dissipation. The amount of energy that the system absorbs from the total input energy (E_i) of the cyclic loading is indicated by the energy dissipation (E_d) value. In the context of a structure's non-linear response, initial stiffness is defined as the ratio of lateral force to deformation under elastic conditions (prior to yielding), whereas secant stiffness is the ratio of lateral force to deformation at the maximum state [36].

Table 1. Results of capacity of the 2D in-plane wall obtained from experimental tests

Parameter	Push		Pull	
	V (kN)	d (mm)	V (kN)	d (mm)
Yield	68.02	13.83	77.81	14.61
Maximum	102.14	31.65	115.86	31.77
Ductility ($\mu = d_{maximum}/d_{yield}$)	-	2.29	-	2.17
at drift 0.50%	69.82	14.46	77.34	14.43
Initial Stiffness (kN/mm)	-	4.92	-	5.33
Secant Stiffness (kN/mm)	-	3.23	-	3.65

In this study, ductility is specifically defined as the ratio of displacement at maximum load to displacement at yield point. The computed ductility ratios for the push and pull directions are 2.29 and 2.17, which range from 2.00 to 3.00. They are classified in the range of limited to moderate ductility, according to the AS 1170.4:2024 standard [37]. The ductility value of 2.17 is not offered as a universal ductility classification parameter since the test was stopped at a drift ratio of 3.00% and the initial experimental dataset does not demonstrate a distinct code-defined collapse or ultimate displacement. Rather, it is only presented as a displacement-based ductility index for the tested object that was obtained through experimentation.

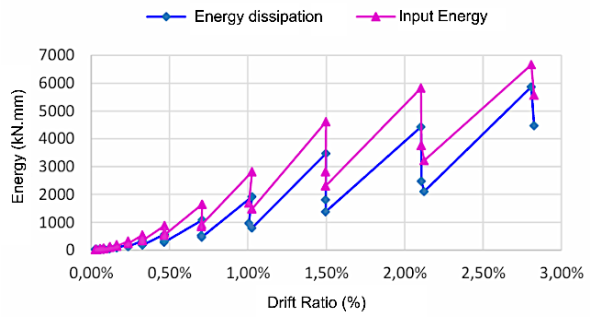
Table 2. Energy dissipation and cumulative energy dissipation

Drift ratio (%)	E_d (kN·mm)	E_i (kN·mm)	E_d/E_i (%)	Cumulative of E_d	Cumulative of E_i
0.13%	48.00	88.83	54.04	439.97	686.59
0.25%	120.16	232.39	51.71	1191.31	1990.38
0.50%	276.41	541.05	51.09	3086.84	5279.56
1.10%	1913.57	2823.07	67.78	7080.18	11531.90
1.60%	1382.38	2300.79	60.08	15509.39	24437.16
2.25%	2478.11	3752.86	66.03	22412.39	34010.35
3.00%	5868.79	6662.18	88.09	30382.73	43894.59

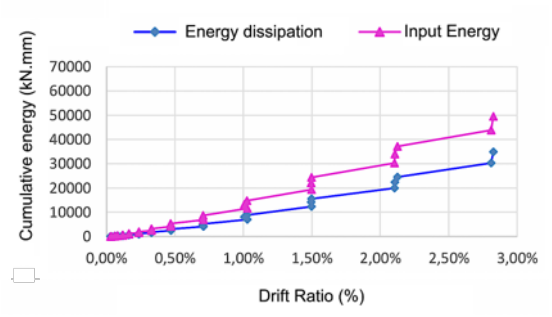
Table 2 and Figure 15 present the values of input energy (E_i), dissipated energy (E_d), and cumulative energy experienced by the test specimen. According to Table 2, the input energy drops from 2,823.07 to 2,300.79 kN·mm over the same drift levels, whereas the dissipated energy drops from 1,913.57 kN·mm at 1.10% drift to 1,382.38 kN·mm at 1.60% drift. As a result, drift does not cause the energy related to individual loading levels to grow monotonically. On the other hand, because they reflect the accumulated energy over subsequent loading cycles, the cumulative dissipated and input energies often rise as the loading history advances. Because they rely on the properties of the related force-displacement hysteresis loops, variations in the energy associated with individual drift levels are expected.

The increase in E_i reflects the greater amount of energy introduced into the structural system as the cyclic load amplitude increases in successive cycles. Meanwhile, the rise in E_d demonstrates the specimen's ability to dissipate energy through inelastic behavior, primarily via progressive yielding of its components. This mechanism continues to develop with increasing cycles until failure occurs.

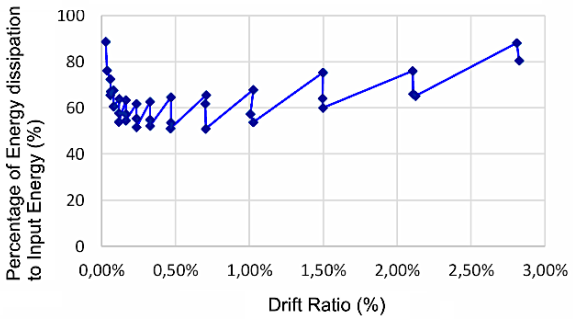
For the computation process, the area enclosed by the corresponding force-displacement hysteresis loop is used to calculate the dissipated energy for each loading cycle, and the sum of the dissipated energies of all completed cycles across the applied loading history yields the cumulative dissipated energy. The force-displacement integration method is used to reliably analyze the input energy. This computation yields a total dissipated energy of 30,382.73 kN·mm at a drift level of 3.00%.



(a) Trend of E_d and E_i



(b) Cumulative E_d and E_i



(c) Percentage of energy dissipation to input energy

Fig. 15. Summary of calculation of Ed and Ei for each testing cycle [12]

The seismic demand used in the demand-to-capacity ratio (DCR) analysis is represented by the equivalent static earthquake base shear force (V) calculated using Equation (1). In this study, 38 representative locations were considered to determine the corresponding values of (V) based on the seismic parameters specified in [7,14]. These locations encompass three site classes: hard soil (SC), medium soil (SD), and soft soil (SE), thereby representing variations in seismic demand associated with different local soil conditions.

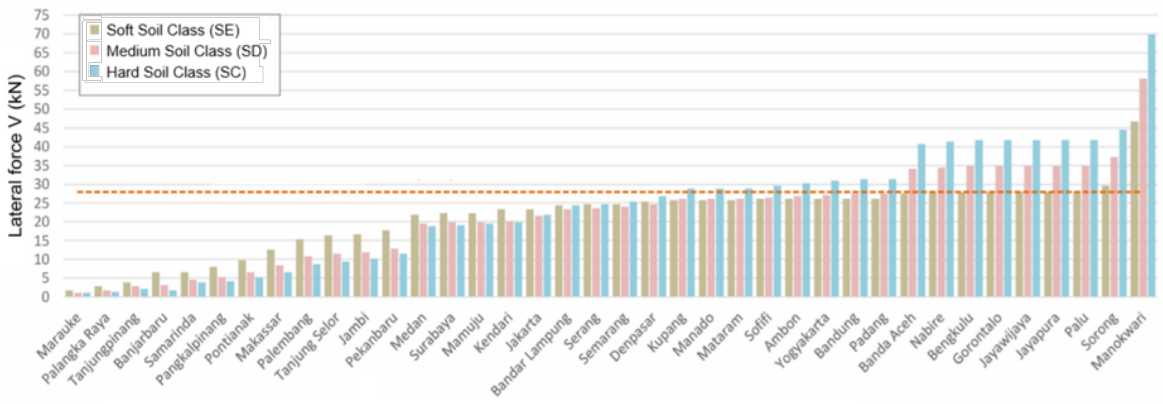


Fig. 16. Graphical presentation of Demand versus Capacity Ratio (DCR)

The structural system is considered to have adequate in-plane shear resistance when $V_{capacity} \geq V$, or equivalently, when the DCR value is less than or equal to 1. Figure 16 presents a graphical evaluation of the DCR results. Based on this analysis, the in-plane DCR of the wall is deemed adequate for locations with SDS ≤ 0.80g.

Under the specific wall configuration according to Figure 9 and the loading assumptions, conservative capacity treatment, and seismic-demand cases evaluated in this research, the tested wall configuration satisfies the adopted in-plane DCR criterion for the evaluated cases with SDS ≤ 0.80g.

3.2 Results of Numerical Analysis

The structural analysis was conducted using the following material properties: concrete compressive strength of 19.02 MPa, modulus of elasticity of concrete of 20,498 MPa, compressive strength of interlocking brick of 14.47 MPa, modulus of elasticity of reinforcing steel of 200,000 MPa, yield strength of reinforcing steel of 353.91 MPa, and ultimate strength of reinforcing steel of 527.89 MPa [13]. Based on these parameters, the 2D in-plane wall model was developed as shown in Figure 17. The numerical modeling adopts an approach in which Columns A and B (Figure 9) are represented as equivalent columns using frame elements. Additionally, Rebar C (Figure 9) and the horizontal reinforcement at an elevation of +3.00 m are modeled as truss (axial-only) elements.

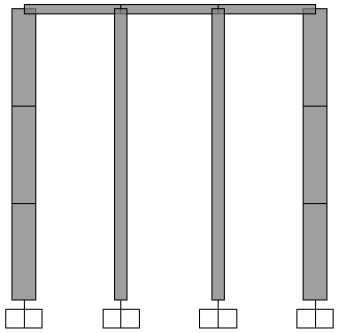


Fig. 17. Finite element model of the 2D in-plane wall PIB prototype

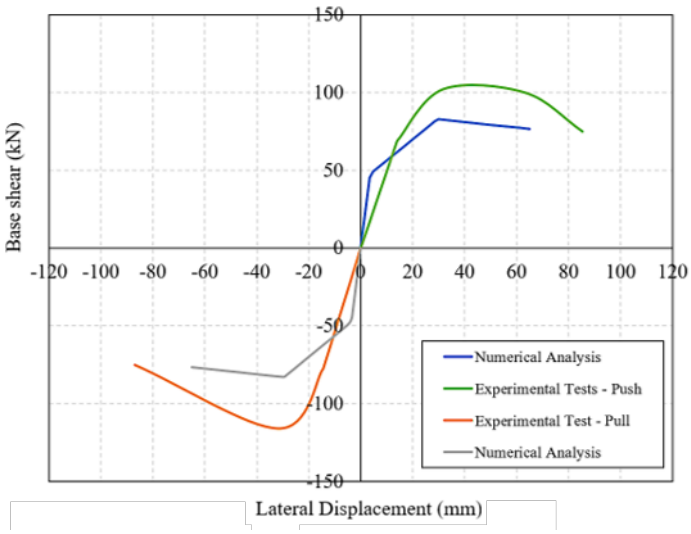


Fig. 18. The load-to-lateral deformation relationship curves obtained from pushover analysis and experimental tests

Table 3. Calculation of the lateral capacity

Results	V_{yield} (kN)	d_{yield} (mm)	$V_{maximum}$ (kN)	$d_{maximum}$ (mm)	Ω_o	$V_{capacity}$ (kN)
Experimental - Push	68.02	13.83	102.14	31.65	2.5	40.86
Experimental - Pull	77.81	14.61	115.86	31.77	2.5	46.34
Numerical model	48.93	5.50	82.80	31.20	2.5	33.12

The analysis was conducted using SAP2000 [11], in which nonlinear hinges (Figure 5) were assigned at the ends of structural elements to capture nonlinear behavior under incremental pushover loading. This approach enables the simulation of inelastic response as the applied lateral load increases progressively from zero to failure. The results of the pushover analysis were used to estimate the structural capacity of the in-plane wall under incremental lateral loading. Figure 18 presents a summary of the results in the form of a capacity curve derived from the numerical model.

However, the analysis has certain limitations, particularly in representing the post-elastic response. This limitation arises from the simplified nonlinear modeling approach, which cannot fully capture complex inelastic material behavior compared to the advanced nonlinear finite element analysis. Although the software is capable of solving nonlinear incremental problems using user-defined load steps and convergence tolerances, it does not incorporate load–displacement control (arc-length method) to trace the structural response up to collapse. Table 3 summarizes the lateral capacity results.

Based on the experimental test results (Table 1), the initial stiffness is calculated to be 4.92 kN/mm (push) and 5.33 kN/mm (pull), while the secant stiffness is found to be 3.23 kN/mm (push) and 3.65 kN/mm (pull). Meanwhile, based on the numerical analysis results presented in Table 3, the initial stiffness is calculated as 8.90 kN/mm and the secant stiffness as 2.65 kN/mm.

As shown in Figure 18, the numerical analysis exhibits a lower capacity curve compared to the experimental envelope curve (i.e., the lower bound of push and pull responses), indicating a more conservative prediction of structural performance.

3.3 Discussion

The lower measured peak load of 102.14 kN is used for conservative evaluation; it is explicitly identified as the governing lower-direction experimental peak rather than the overall maximum experimental load. Structural design for earthquake loading is critically important, particularly for buildings located in high seismic zones and subjected to earthquakes exceeding moment magnitude (Mw) 6.0 [38, 39]. This is because structural stiffness is significantly influenced by lateral loads induced during seismic events. Excessive deformation not only causes discomfort to occupants but may also lead to permanent structural damage once the response enters the post-elastic range.

Significant inelastic lateral deformation can result in damage that is no longer economically repairable and may also compromise non-structural components. Therefore, design codes impose limits on allowable drift to control damage levels. For instance, FEMA P-2082-1 [40] specifies an allowable story drift of 0.70% for masonry shear walls. The Peruvian Design Code [41] limits the drift ratio for masonry structures to 1/200 (0.50%) to ensure that damage remains repairable. Similarly, ACI 374.2R-13 [42] defines the Immediate Occupancy performance level for structural walls as a drift ratio not exceeding 0.50% under lateral loading.

4. Conclusions

The conclusions obtained from the research are as follows:

- The results indicate that the capacity curves obtained from numerical analysis exhibit trends similar to those observed in the experimental tests.
- The numerical analysis result show a maximum load capacity of 82.80 kN, which is 18.93% lower than the experimental results (V_{max}) of 102.14 kN.
- The stiffness behavior yields a ductility factor of 2.17, classifying the structure as having a range from limited to moderate ductility criteria.
- The energy dissipation capacity was recorded at 30,382.73 kN·mm.
- In response to the growing demand for housing, PIB technology provides an efficient approach that enables rapid construction while maintaining structural quality in accordance with Indonesian national standards. The current results should be viewed as preliminary experimental data rather than a straight call for quick code modification when it comes to inclusion into design standards. First, design-oriented analytical models can be calibrated using the measured backbone curve, stiffness, ductility, energy dissipation, and lateral resistance.
- The present DCR results provide an initial application range in which the tested two-dimensional inplane PIB prototype satisfied the adopted strength criterion for SDS ≤ 0.80g. This does not establish the seismic adequacy of a complete three-dimensional PIB building. Effects of wall distribution, torsion, diaphragm action, orthogonal walls, openings, connections, foundations, gravity loading, redundancy, and out-of-plane response remain outside the present scope.

Acknowledgement

This research was funded by PT Semen Indonesia (Persero) Tbk (SIG) for the 2024 and 2025 fiscal years.

References

[1] Argalis PP, Gelzis K, Valdovskis RK, Vitola L. Comparative analysis of industrial waste as supplementary cementitious materials - a preliminary study. Recycling. 2026;11:75. https://doi.org/10.3390/recycling11040075

[2] Susilawati, Tyas IW. Lock-brick system for sustainable and environment infrastructure building materials. IOP Conf Ser Mater Sci Eng. 2018;371:012016. https://doi.org/10.1088/1757-899X/371/1/012016

[3] Yuhanah T, Mayasari D, Iduwin T. Eco-friendly concrete with high initial compressive strength using recycled concrete, silica fume and superplastiser. J Sustain Innov Eng. 2025;1(1):27-33.https://doi.org/10.69693/sustainable.v1i1.5
[4] Khan ZI, Habib U, Mohsin MEA, Younas MY, Mohamad Z. Synergistic HNT/GNP reinforcement in compatibilized RPET/PA-11 hybrid nanocomposites: Simultaneous gains in mechanical and thermal properties. Polym Int. 2026.
[5] Rasidi N, Rochman T, Sumardi S, Purnomo F. Structural behavior of lightweight interlocking brick system. IOP Conf Ser Mater Sci Eng. 2020;732:012026. https://doi.org/10.1088/1757-899X/732/1/012026
[6] Wang G, Zhang X, Hao XH, Li G. Dynamic response of reinforced interlocking brick wall under impact loading.Int J Impact Eng. 2025;204:105388. https://doi.org/10.1016/j.ijimpeng.2025.105388
[7] National Standardization Agency. SNI 1726:2019 Procedures for design of earthquake resistance of building and non-building structures. Jakarta: National Standardization Agency; 2019.
[8] National Standardization Agency. SNI 2847-2019 Structural concrete requirements for buildings. Jakarta: National Standardization Agency; 2019.
[9] National Standardization Agency. SNI 1727:2020 Minimum design loads and related criteria for buildings and other structures. Jakarta: National Standardization Agency; 2020.
[10] ASTM International. ASTM E2126-19 Standard test methods for cyclic (reversed) load test for shear resistance of vertical elements of the lateral force resisting systems for buildings. West Conshohocken (PA): ASTM International; 2019.
[11] Computers and Structures, Inc. SAP2000 finite element software reference. Berkeley (CA): Computers and Structures, Inc.; 2023.
[12] Semen Indonesia Group. 2D precise interlock brick testing report. Gresik: PT Semen Indonesia (Persero) Tbk.; 2024.
[13] Semen Indonesia Group. 2D wall cyclic test of precise interlock brick (PIB). Gresik: PT Semen Indonesia (Persero) Tbk.; 2025.
[14] PusGeN. Indonesia spectra design 2021. Cileunyi: Center for Settlement Research and Development, Ministry of Public Works and Housing; 2021.
[15] Khan ZI, Othman N, Germaine LYL, Low JT, Mohamad Z, Wahit MU, et al. Structural, mechanical, and physicochemical characterization of regenerated silk fibroin/cellulose composite films fabricated through ionic liquid dissolution. Biomater Transl. 2026;0(0):279.
[16] Abdullah NAS, Mohamad Z, Khan ZI. Thermo-mechanical properties and optimization of sodium alginate as a polymer backbone substrate for biosensor application. Environ Qual Manag. 2024;34(1):1-11.https://doi.org/10.1002/tqem.22242
[17] Rosmmi NHM, Khan ZI, Mohamad Z, Majid RA, Othman N, Man SHC, et al. Impact strength and morphology of sustainably sourced recycling polyethylene terephthalate blends. Chem Eng Trans. 2021;83:266-70.
[18] National Standardization Agency. SNI 7064:2014 Composite portland cement. Jakarta: National Standardization Agency; 2014.
[19] ASTM International. ASTM C33/C33M-23 Standard specification for concrete aggregates. West Conshohocken (PA): ASTM International; 2023.
[20] Pranata YA, Wiyono DR, Sabaruliman AAG, Saputra YA, Rakhman J, Milyardi M. Seismic behavior of modular precast concrete with a base isolation device system for healthcare facilities. Civ Eng Archit. 2026;14(5):3914-29.https://doi.org/10.13189/cea.2026.140534
[21] Gupta A, Singhal V. Experimental investigation of confined masonry walls with openings. J Struct Eng.2024;150(10):13305. https://doi.org/10.1061/JSENDH.STENG-13305
[22] Xie G, Zhang X, Hao H, Shi T, Cui L, Thomas J. Behaviour of reinforced mortarless interlocking brick wall under cyclic loading. Eng Struct. 2023;283:115890. https://doi.org/10.1016/j.engstruct.2023.115890
[23] National Standardization Agency. SK SNI T-15-1991-03 Procedures for calculating concrete structures for buildings. Jakarta: National Standardization Agency; 1991.
[24] Federal Emergency Management Agency. FEMA P-750 National earthquake hazards reduction program recommended seismic provisions for new buildings and other structures. Washington (DC): Federal Emergency Management Agency; 2009.
[25] Mimeouni M, Kerdal DED, Kharroubi L. Numerical study of stiffness degradation and dissipated energy in early cyclic behavior of non-conforming RC beam-column joints. Res Eng Struct Mater. 2026;12(2):845-57.https://doi.org/10.17515/resm2026-1316st1102rs
[26] Ebenezer SJ, Tensing D, Jebadurai SS. An experimental study on composite steel encased portal frame under cyclic loading. Res Eng Struct Mater. 2023;9(1):277-91.
[27] Ridha IH, Al-Abbas BH, Hemzah SA. Effect of different reinforcement methods on column-footing joint performance under seismic loading. Res Eng Struct Mater. 2026;12(2):1127-37. https://doi.org/10.17515/resm2026-1312ic1031rs

[28] Senthil K, Rupali S, Satyanarayanan KS. Experiments on ductile and non-ductile reinforced concrete frames under static and cyclic loading. J Coupled Syst Multiscale Dyn. 2017;5(1):38-50. https://doi.org/10.1166/jcsmd.2017.1118
[29] Arafat AMA, Suci IM, Alie MZM. The analysis of 2D frame structure subjected to point load. IOP Conf Ser Earth Environ Sci. 2020;575:012204. https://doi.org/10.1088/1755-1315/575/1/012204
[30] Sakr MA, El-Khoriby SR, Seleemah AA, Aboelnour MM, Osama B. Experimental and numerical investigation on cyclic behavior of masonry infilled RC frames retrofitted with partially bonded CFRP strips. Structures. 2021;33:2238-52. https://doi.org/10.1016/j.istruc.2021.05.087
[31] Tekkaya AE, Soyarslan C. Finite element method. In: Chatti S, Laperrière L, Reinhart G, Tolio T, editors. CIRP Encyclopedia of Production Engineering. Berlin: Springer; 2019. p. 508-14. https://doi.org/10.1007/978-3-642-20617-7_16699
[32] Morita N. Finite element methods. Cham: Springer Nature; 2021. https://doi.org/10.1016/B978-0-323-91112-2.00004-5
[33] Ren LX. Factors affecting the mechanical properties of precast concrete infill walls. Int J Eng Technol Innov.2025;15(4):456-75. https://doi.org/10.46604/ijeti.2025.15418
[34] Bertrand D, Grange S, Charrie JB. Progressive collapse analysis of RC frame building based on pseudo-dynamic (PsD) testing with sub-structuring. J Build Eng. 2022;52:104420. https://doi.org/10.1016/j.jobe.2022.104420
[35] Guettala S, Abdesselam I, Rahmani AY, Khelaifia A, Guettala S. Advancements in pushover analysis for improved seismic performance evaluation review. Arch Comput Methods Eng. 2025;32:4525-54. https://doi.org/10.1007/s11831-025-10278-9
[36] Sullivan TJ, Calvi GM, Priestley MJN. Initial stiffness versus secant stiffness in displacement-based design. In:Proceedings of the 13th World Conference on Earthquake Engineering; 2004 Aug 1-6; Vancouver, Canada. 2004.
[37] Standards Australia. AS 1170.4 Structural design actions, Part 4: Earthquake actions in Australia. Sydney:Standards Australia; 2024.
[38] Bellido NG, Aguilar Z. Seismic performance of a tailings dam located in high seismicity area. ASEAN J Sci Eng.2024;4(3):511-36. https://doi.org/10.17509/ajse.v4i3.75557
[39] Khurram S, Khalid P. Moment tensor components with their corresponding eigenvalues and eigenvectors for earthquakes MW ≥ 6.0 in northern and southwestern of Pakistan. ASEAN J Sci Eng. 2021;1(2):79-96.https://doi.org/10.17509/ajse.v1i2.34950
[40] Federal Emergency Management Agency. NEHRP recommended seismic provisions for new buildings and other structures, Volume I: Part 1 provisions, Part 2 commentary (FEMA P-2082-1). Washington (DC): Federal Emergency Management Agency; 2020.
[41] Peru Japan Center of Seismic Research and Disaster Mitigation. Technical standard of building E.030:Earthquake-resistant design (NTE E.030). Vienna: United Nations Office for Outer Space Affairs; 2003.
[42] American Concrete Institute. ACI 374.2R-13 Guide for testing reinforced concrete structural elements under slowly applied simulated seismic loads. Farmington Hills (MI): American Concrete Institute; 2013.